

On the selection of models for the high-frequency quasiperiodic oscillations of black holes: The mass problem

Ivan Zh.Stefanov[★] and Radostina P. Tasheva

Department of Applied Physics, Technical university of Sofia, 8, Snt. Kliment Ohridski Blvd., 1000 Sofia, Bulgaria

Accepted XXX. Received YYY; in original form ZZZ

ABSTRACT

High-frequency quasiperiodic oscillations of the X-ray flux coming from black-hole binaries have the potential to provide precise estimates of the mass and the spin of the central black hole, if an adequate model for them was available. There are several models in the literature but none of them is commonly accepted. One way to test the available models is to confront their predictions for the masses of black holes with results obtained through other methods. Here, we study the mass bounds that nine of the most commonly used models provide for the three microquasars with known masses GRS 1915+105, GRO 1655-40 and XTE 1550-564 which display high-frequency quasiperiodic oscillations in their X-ray spectra. We also propose a statistical method for the assessment of the average success of the models. The results allow us to discard five of them. Here, "the mass problem" designates the conflict between their predictions and the reference masses.

Key words: black hole physics – relativistic processes – accretion, accretion discs – stars: black holes – X-rays: individuals: GRS 1915+105, GRO 1655-40, XTE 1550-564

1 INTRODUCTION

Quasiperiodic oscillations of the X-ray flux coming from black-hole binaries have been demonstrated to serve as a very precise method for the estimation of the mass and the spin of the central black hole. Recently [Motta et al. \(2014a\)](#) applied the relativistic precession model to provide very precise estimates of the mass and the spin of the central object in the low-mass X-ray binary GRO 1655-40. An alternative study of the same object based on the same model was conducted by [Bambi \(2013\)](#). It confirmed the results of the former work.

Which circumstances made this possible? The suitable choice of a model for the QPOs, the suitable choice of a metric of the spacetime, and the rare event of a simultaneous observation of C-type low-frequency QPOs and a pair of twin (a lower and an upper) high-frequency QPOs. The choice of a model and metric, however, are far from unique. Even if we agreed not to question the Kerr metric, we would still face many uncertainties. One of the major difficulties with the application of the QPOs for the measurement of the basic parameters of black holes, mass and spin, is the absence of a verified and, hence, commonly accepted model for the HF QPOs.

How could we test the different models for the HF QPOs

and discard the improper ones? If sufficiently large observational data sets were available we could apply statistical tests to evaluate the models and reject the bad ones. Examples of such studies for the case of kHz QPOs, which are the analogues of HF QPOs for neutron stars, can be found in [Lin et al. \(2011\)](#); [Török et al. \(2012, 2016\)](#). The situation with black holes is less favorable, since the HF QPOs observed in their power density spectra are very faint. As a result, HF QPOs are observed for a small number of black holes [van der Klis \(2006\)](#); [McClintock & Remillard \(2006a\)](#); [Remillard & McClintock \(2006a\)](#); [Zhang \(2013\)](#); [Zhou et al. \(2015\)](#); [Pasham et al. \(2013\)](#). Twin HF QPOs are even rarer. What is even worse, for most of these objects, unlike the situation with the kHz QPOs of neutron stars, only a single pair of twin HF QPOs is seen. So, it appears that no statistical testing is possible.

An alternative approach for the verifications of the models for the HF QPOs is to confront their predictions with facts that have been ascertained by other methods. Examples can be found in ([Török et al. 2011](#)) and ([Török et al. 2007](#)). These studies compare the constraints of the models for the HF QPOs on the spin of the black holes on the one side, to the values coming from other methods such as the fitting of the continuum of the X-ray spectrum and the fitting of the asymmetric profile of the $K\alpha$ iron line, on the other side. A conflict between values obtained by the differ-

[★] E-mail: izhivkov@tu-sofia.bg

ent methods has been ascertained. This conflict is termed “the spin problem” (See also [Rebusco \(2008\)](#)).

One of the caveats of the cited studies based on the comparison of predictions for the spin is the fact that they use the masses of the objects obtained through dynamical observations as input parameters. This is a possible source of uncertainty. Another potential problem is the fact that the different methods for the measurement of the spin of the black holes might give conflicting results and one is not sure which value to take as a reference. Different estimates for the spin of GRS 1915+105, for example, can be found in ([McClintock et al. 2006b](#); [Blum et al. 2009](#); [Middleton et al. 2006](#)).

In this work we propose a different approach. It is based on the comparison of the constraints that different methods impose on the mass, instead of the spin, of the black holes. What values do we use for the spin? An upper boundary on the spin comes from theory – it cannot be greater than one. A lower bound on the spin can be obtained from the LF QPOs present in the spectra of the studied objects – they originate in the accretion disk and are thus related to orbits which are outside of the innermost stable circular orbit (ISCO). To our knowledge, this condition has been applied for the first time in [Schnittman et al. \(2006\)](#) to obtain lower bounds on the spin. It has been later applied in ([Stefanov 2014](#)) to test the models of the HF QPOs. Recently, [Franchini, Motta & Lodato \(2017\)](#) used LF QPOs in a similar manner to constrain the spins of black holes.

Using the bounds on the spin we obtain bounds on the mass. The latter are confronted with the reference values obtained through dynamical observations. The idea that the confrontations of the predictions of the models for the HF QPOs for the masses of the observed black holes on the one side, with the dynamically obtained masses on the other side, are an indication of a bad model has been exploited by [Stuchlík & Kološ \(2016a\)](#). They applied it to the microquasar GRO 1655-40. A possible outcome of the ascertained conflicts was proposed by the same authors in ([Stuchlík & Kološ 2016b](#)).

It appears that the mass constraints coming from some models for the HF QPOs fail to explain the observed masses. Can these failures be attributed to random effects? In attempt to find an answer to this question we propose a method for the measurement of the “average success” of the models. In brief, we find the average position of the observed masses in the intervals that a given model provides for a sample of (only) three objects. In order to allow averaging we project all mass intervals to the unit interval. Then we evaluate the average position of the projected observed masses. If it is outside of the unit interval, then failures are either too big or occur too often or both, and we have serious reason to question the viability of the given model.

The test that we propose requires black holes with known masses the power density spectra of which have the following components: C-type LF QPOs¹ and a pair of twin HF QPOs. To our knowledge, there are only three microquasars which meet this requirements: GRS 1915+105, GRO 1655-40 and XTE 1550-564. The masses of their black holes,

the frequencies of the LF and HF QPOs and references for them are given in Table 1.

2 MODELS FOR THE HF QPOS

Most hypotheses concerning the origin of QPOs assume a direct connection between the QPO frequencies and the fundamental frequencies of motion of matter orbiting black holes (BH). The models which consider either “hot spot” or “disk oscillation” modes comprise two large groups – relativistic precession (RP) and resonant models. The frequencies that the different models attribute to the observed lower and upper HF QPOs are summarized in Table 2.

2.1 Relativistic precession model (RP)

The precession models predict QPOs excitation from a variety of resonances between the precession and the orbital frequencies under certain conditions, for example inhomogeneities orbiting close to the inner disk boundary.

The relativistic precession model proposed by [Stella & Vietri \(1998\)](#), [Stella, Vietri & Morsink \(1999\)](#) and [Merloni et al. \(1999\)](#) explains the twin HF QPOs as a result of relativistic epicyclic motion of radiating hot blobs traveling along orbits with different radii r in the inner part of the accretion disk. Their correlation can be attributed to the periastron precession of the relativistic orbits occurring in the strong gravity field in the vicinity of BH. This model associates the upper of the twin HF QPOs with the orbital frequency, $\nu_U = \nu_\phi$ ². The lower one is attributed to the periastron precession frequency, $\nu_L = \nu_{\text{per}} = \nu_\phi - \nu_r$. To match the observed 3:2 ratio the HF QPOs have to be generated very close to the ISCO. According to authors of the relativistic precession model the LF QPOs are a result of Lense-Thirring precession³ with nodal frequency $\nu_{\text{nod}} = |\nu_\phi - \nu_\theta|$. On the dependence between LF and HF QPOs we refer the reader also to ([Belloni, Psaltis & van der Klis 2002](#)). The relativistic precession model is successful in explanation of this relation for a number of neutron stars and black holes ([van der Klis 2006](#)). These models, however, do not provide generic explanations for the observed 3:2 frequency ratio $R=3/2$ of the twin HF QPOs. Hence, it is a good idea to explore, if some orbits are preferred to others.

² See appendix A for the explicit form of the frequencies met in this section.

³ The idea that C-type LF QPOs have geometric origin is supported by the original papers of the authors of the RP model ([Stella & Vietri 1998](#)), ([Stella, Vietri & Morsink 1999](#)). There is a number of studies in the context of neutron stars that question this interpretation (See, for example, ([Altamirano et al. 2012](#))). A recent example is the thorough research conducted by [van Doesburgh & van der Klis \(2017\)](#). Instead of one, they found several frequencies in the low-frequency sector that could be identified as LF QPOs. Frame dragging, i.e. Lense-Thirring precession, could explain the presence of only one them.

¹ We refer the reader to ([Casella et al. 2005](#)) and ([Motta 2016](#)) for the classification of LF QPOs.

Table 1. Data for the studied black holes

source	M/M_{\odot}	ν_{LF} , [Hz]	ν_{L} , [Hz]	ν_{U} , [Hz]	Ref.
GRS 1915+105	$12.4^{+2.0}_{-1.8}$	10	113 ± 5	168 ± 3	1, 2, 3, 4
XTE 1550-564	9.1 ± 0.6	10 (18) ^a	184 ± 5	276 ± 3	5, 6, 7, 8
GRO 1655-40	5.4 ± 0.3^b	28	300 ± 5	450 ± 3	9, 10, 11

References in Table 1: 1 Reid et al. (2014), 2 Hurley et al. (2013), 3 Morgan et al. (1997), 4 McClintock et al. (2006b), 5 Orosz et al. (2011), 6 Sobczak et al. (2000), 7 Remillard et al. (2002a); 8 Remillard et al. (2002b), 9 Beer & Podsiadlowski (2002), 10 Remillard (1999), 11 Strohmayer (2001).

^a The greater value, 18 Hz, is taken from Sobczak et al. (2000) in which the classification of the LF QPOs is not stated. This paper was published before the ABC classification of the LF QPOs had been invented.

^b An alternative estimate of the mass of GRO 1655-40, $6.30 \pm 0.27 M_{\odot}$, is given in (Orosz 2003; Shafee 2006)

Table 2. Models for the HF QPOs.

Model	ν_{L}	ν_{U}
3:2	ν_{r}	ν_{θ}
3:1	$\nu_{\theta} - \nu_{\text{r}}$	ν_{θ}
2:1	ν_{θ}	$\nu_{\theta} + \nu_{\text{r}}$
3:2 K	ν_{r}	ν_{ϕ}
3:1 K, RP	$\nu_{\phi} - \nu_{\text{r}}$	ν_{ϕ}
2:1 K, TD	ν_{ϕ}	$\nu_{\phi} + \nu_{\text{r}}$
RP1	$\nu_{\phi} - \nu_{\text{r}}$	ν_{θ}
RP2	$\nu_{\phi} - \nu_{\text{r}}$	$2\nu_{\phi} - \nu_{\theta}$
WD	$2(\nu_{\phi} - \nu_{\text{r}})$	$2\nu_{\phi} - \nu_{\text{r}}$

2.2 Tidal disruption model (TD)

Another “hot spot” model is the tidal disruption model (TD), where hot orbiting clumps distorted by the tidal forces of the black hole and forming “ring-like” segments are responsible for the observed modulation of the power density spectra (Cadez et al. 2008; Kostic et al. 2009; Germana et al. 2009). The TD model implies that $R \in (1, 2)$ for any spin of the black hole and radius of the orbit but still does not firmly constrain the ratio of the twin HF QPO (Török et al. 2011). The Roche radius r_{TD} is the distance where tidal forces start to disrupt an approaching object. Its upper limit for a fluid body with density ρ orbiting a massive body with mass M is $\propto (M/\rho)^{1/3}$. The corresponding frequency according to Kepler’s third law is $\nu_{\text{TD}} \propto (GM/r_{\text{TD}})^{1/2}$. After r_{TD} is replaced ν_{TD} is proportional to $(G\rho)^{1/2}$. As a result $\nu_{\text{L}} = \nu_{\text{TD}} \propto 10^{-3}\text{Hz}$, which is much lower than the observed 100 Hz frequency. Nevertheless, the authors of this model managed to obtain plausible light curves and to fit the HF part of power density spectra of the low mass X-ray binary XTE 1550-564. Moreover, with this model they were able to mimic the twin HF QPOs.

2.3 Warped disk model (WD)

Kato introduced for the first time the warped disk resonance model which proposes an excitation mechanism for the orbiting particle oscillations (Kato 2004a,b; Kato 2005a;

Kato 2005b, 2007). The internal viscid and adiabatic perturbations of a deformed accretion disk lead to a horizontal resonance responsible for HF QPOs. The model is successfully applied to estimate the mass and angular momentum of LMXB GRS 1915+105 (Kato 2004c).

2.4 RP1 and RP2 - improved precession models

These models are versions of the precession models, i.e. the QPOs are supposedly excited by resonances of precession and nonaxisymmetric oscillation modes. They are connected to oscillation modes whose frequencies attributed to slow rotation coincide with the frequencies predicted by RP model. In the case of RP1 the rotating fluid torus has slight eccentricity and its vertical oscillations are superimposed on the precession modes to finally form the emitted radiation flow (Bursa 2005). The author expresses the lower frequency as the relativistic periastron precession frequency $\nu_{\text{L}} = \nu_{\text{per}} = \nu_{\phi} - \nu_{\text{r}}$, while the upper one is hypothesized as $\nu_{\text{U}} = \nu_{\theta}$. The RP2 model according to Török et al. (2011) and Török et al. (2012) is based on perturbations, where ν_{ϕ} is not the dominant frequency. HF QPOs are produced by the resonance between radial and vertical modes. The RP1 model can explain the twin HF QPOs in XTE 1550-564 (Török et al. 2011). It also gives reasonable explanation of the QPOs in GRO J1655-40 and provides results similar to (Motta et al. 2014a).

2.5 Nonlinear resonance models (NRM)

There are two types of resonant disk oscillation models – the epicyclic resonance and the warped disk oscillation (WD) models. Resonant epicyclic models of the twin HF QPOs (Abramowicz & Kluzniak 2004; Abramowicz et al. 2004; Török et al. 2006) suggest resonance between the fundamental oscillation modes of the accretion disk. The assumed resonance is either parametric, or a nonlinearly forced one. The model predicts that one of the frequencies $\nu_{-} = \nu_{\theta} - \nu_{\text{r}}$ and $\nu_{+} = \nu_{\theta} + \nu_{\text{r}}$ is in 3:2 ratio with the vertical frequency ν_{θ} . For $\nu_{\theta} : \nu_{\text{r}} = 2 : 1$, $\nu_{\text{L}} = \nu_{\theta}$, $\nu_{\text{U}} = \nu_{+} = \nu_{\theta} + \nu_{\text{r}}$. For $\nu_{\theta} : \nu_{\text{r}} = 3 : 1$, $\nu_{\text{L}} = \nu_{-} = \nu_{\theta} - \nu_{\text{r}}$, $\nu_{\text{U}} = \nu_{\theta}$. The commensurability of the frequencies is crucial for the NRM mod-

els. Although attractive for their simplicity these models cannot provide an adequate mechanism for the excitation of the QPOs⁴. There is also a discrepancy (Török et al. 2007; Rebusco 2008) between their predictions for the angular momenta and measurements based on other methods such as: jet emission analysis, analysis of the profile of the K_α iron line and spectral continuum fitting. We refer the reader to (Aliev, Esmer & Talazan 2013) and (Bambi 2012) for applications of the NRM to Kerr and non-Kerr black holes, respectively. Nonlinear resonances occurring in the field of braneworld Kerr black holes and Kerr super-spinars (i.e. Kerr naked singularities) have been studied in (Stuchlik & Kotrlova 2009) and (Stuchlik & Schee 2012).

2.6 Keplerian nonlinear resonance model

The Keplerian nonlinear resonance model differs from the epicyclic NRM in its prescription for the upper frequency of the HF QPOs. In the former model $\nu_U = \nu_\phi$ instead of $\nu_U = \nu_\theta$.

3 METHOD FOR THE ATTAINING OF THE MASS BOUNDS

The method that we apply to obtain loose bounds on the mass of the central object in black-hole binaries has been proposed first in (Stefanov 2014) but is presented in the current section in a different way. It has been designed for the Kerr metric (and takes advantage of the qualitative behavior of the fundamental frequencies of test particles and other function derived from them) but could be generalized also to other black-hole spacetimes which are parameterized by two parameters. In the case of Kerr spacetime the two parameters are mass M and specific angular momentum (or spin) a .

The main idea of the method is to pose constraints on the spin of the black hole and use the mass-spin relation resulting from a model for the HF QPOs to constrain the mass.

An upper bound on the specific angular momentum comes from the theory of the Kerr black hole – it cannot be greater than one. The observation of a pair of simultaneous HF QPOs allows us to express the mass of the black hole as a function of the spin. With this metric and for the set of models considered here this function is monotonous. It is increasing (decreasing) in the case of prograde (retrograde) motion of the hot spot which produces the HF QPOs. Hence, the upper bound on the spin gives a upper (lower) bound on the mass in the prograde (retrograde) case.

The presence of LF QPOs in the X-ray power density spectrum of a LMXB allows us to obtain a lower bound on its angular momentum. The values of the LF QPOs vary significantly with the evolution of the object. According to the RP model LF QPOs result from the Lense-Thirring precession of matter inhomogeneities in the accretion disk, dubbed hot spots. The variance of the frequency values is produced

by the variance of the orbital radii of the hot spots. The frequency of the LF QPOs is associated with the nodal precession frequency $\nu_{\text{nod}} = |\nu_\phi - \nu_\theta|$. If the Kerr metric is assumed the nodal precession frequency is a function of three variables: M , a and r_{LF} , where r_{LF} is the radius of the orbit of the hot spot, i.e. the radius on which the LF QPOs originate. The last parameter can be obtained from the equation

$$\nu_{\text{nod}}(a, M, r_{\text{LF}}) = \nu_{\text{LF}}^{\text{obs}}, \quad (1)$$

in which $\nu_{\text{LF}}^{\text{obs}}$ is an observed value of the LF QPOs. If the mass M of the black hole is known, (1) results in a $a - r_{\text{LF}}$ relation, the radius is an implicitly defined monotonously increasing function of the angular momentum. The radius of the orbit and, hence, the angular momentum cannot be arbitrarily small. A lower bound comes from the natural requirement that the LF QPOs originate at an orbit whose radius r_{LF} is greater than or at least equal to the radius of the innermost stable circular orbit r_{ISCO} . The radius r_{ISCO} is function of a alone, while r_{LF} depends on both a and M . In the limit $a \rightarrow 0$, while M is finite, the radius $r_{\text{LF}}(a, M)$ vanishes and is, hence, lower than $r_{\text{ISCO}}(a)$. For high enough values of the angular momentum $r_{\text{LF}}(a, M) > r_{\text{ISCO}}(a)$. A lower bound on the angular momentum $a_{\text{LF}}^{\text{min}}(M)$ is obtained from the equality $r_{\text{LF}}(a_{\text{LF}}^{\text{min}}, M) = r_{\text{ISCO}}(a_{\text{LF}}^{\text{min}})$. This equation is equivalent to the system composed of (1) and the equation which defines the ISCO

$$\nu_r(a, r_{\text{LF}}) = 0. \quad (2)$$

In general, this system might have two solutions – one for prograde and one for retrograde rotation of the hot spot. Greater values of $\nu_{\text{LF}}^{\text{obs}}$ yield greater lower bounds on the angular momentum. In other words, the greatest observed value of the LF QPOs in the spectrum of a given object gives the most stringent constraint on its $a_{\text{LF}}^{\text{min}}$. The function $a_{\text{LF}}^{\text{min}}(M)$ is monotonously increasing for prograde orbits and monotonously decreasing for retrograde ones.

In case M is unknown $a_{\text{LF}}^{\text{min}}$ is also unknown. The minimum value of $a_{\text{LF}}^{\text{min}}$ which we denote as a_{min} , however, can be found if a pair of twin simultaneous HF QPOs has been observed in the X-ray power spectrum of a given BHB. With the observed HF QPOs one can compose the following algebraic system of equations

$$\nu_L(a, M, r_{\text{HF}}) = \nu_L^{\text{obs}}, \quad (3)$$

$$\nu_U(a, M, r_{\text{HF}}) = \nu_U^{\text{obs}}. \quad (4)$$

The explicit form of $\nu_L(a, M, r_{\text{HF}})$ and $\nu_U(a, M, r_{\text{HF}})$ depends on the choice of a model for the HF QPOs and of a metric. If M is known, the system above can be solved for the angular momentum of the BH a and the radius of the orbit on which the HF QPOs occur r_{HF} . For unknown values of M the system (3)-(4) results in a $a - M$ relation, i.e. the functions $a(M)$ and $r_{\text{HF}}(M)$ are defined implicitly⁵. For the radius and the angular momentum we have also the following constraints: $r_{\text{HF}}(M) \geq r_{\text{ISCO}}(a(M))$ and $a(M) \geq a_{\text{LF}}^{\text{min}}(M)$. The numerical analysis shows that in all cases studied below the former is satisfied. The latter is satisfied only for high (low) enough masses in the case of prograde (retrograde)

⁴ We should mention for the reader, however, that excitation mechanisms (more than one) have been proposed in (Stuchlik et al. 2008).

⁵ The presence of the $a - M$ degeneracy has been noticed in (Török et al. 2010, 2012) and (Stefanov 2016)

motion of the hot spot. The equality gives us a lower (upper) bound on the mass M_{\min} in the prograde (retrograde) case and a lower bound on the angular momentum a_{\min} : $a_{\min} \equiv a(M_{\min}) = a_{\text{LF}}^{\min}(M_{\min})$. Please note that M_{\min} designates the value of mass which minimizes a , not the lower bound of the mass.

To summarize what was said above, a lower bound on the angular momentum a_{\min} of a black hole whose X-ray power density spectrum contains the following triad of frequencies – $\nu_{\text{LF}}^{\text{obs}}$, $\nu_{\text{L}}^{\text{obs}}$ and $\nu_{\text{U}}^{\text{obs}}$, where the last two are simultaneously observed, is obtained from the requirement that $a(M_{\min}) = a_{\text{LF}}^{\min}(M_{\min})$. In general the unknown variables are five – a , a_{LF}^{\min} , M , r_{LF} , r_{HF} , while the equations are only four – (1), (2), (3), (4). In the special case $M = M_{\min}$, however, the relation $a = a_{\text{LF}}^{\min} = a_{\min}$ reduces the number of the unknown variables and it turns out that we can find a_{\min} with the following recipe. The system

$$\frac{\bar{\nu}_{\text{L}}(a_{\min}, r_{\text{HF}})}{\bar{\nu}_{\text{U}}(a_{\min}, r_{\text{HF}})} = \frac{\nu_{\text{U}}^{\text{obs}}}{\nu_{\text{L}}^{\text{obs}}}, \quad (5)$$

$$\frac{\bar{\nu}_{\text{L}}(a_{\min}, r_{\text{HF}})}{\bar{\nu}_{\text{LF}}(a_{\min}, r_{\text{LF}})} = \frac{\nu_{\text{L}}^{\text{obs}}}{\nu_{\text{LF}}^{\text{obs}}}, \quad (6)$$

$$\bar{\nu}_{\text{r}}(a_{\min}, r_{\text{LF}}) = 0. \quad (7)$$

is independent of M . The bar designates the part of the expression for the frequencies that is independent of M

$$\nu_i(a, M, r) = \frac{\bar{\nu}_i(a, r)}{M}, \quad i = \text{U, L, LF, r}. \quad (8)$$

The system (5)–(7) has three equations and three unknowns: a_{\min} , r_{HF} and r_{LF} . It is solved numerically. Once a_{\min} and r_{HF} are found M_{\min} can be obtained from $\nu_{\text{L}}(a_{\min}, M_{\min}, r_{\text{HF}}) = \nu_{\text{L}}^{\text{obs}}$ (or $\nu_{\text{U}}(a_{\min}, M_{\min}, r_{\text{HF}}) = \nu_{\text{U}}^{\text{obs}}$).

4 MASS BOUNDS FOR THE STUDIED OBJECTS

The mass bounds that the different models impose on the studied black holes are given in the current section. They have been obtained with the application of the method described in section 3. There are two mass intervals for each model – for prograde and retrograde orbits, respectively. The lower interval of masses corresponds to retrograde rotation of the inhomogeneities, hot spots or perturbation modes, in the accretion disk. The vertical dotted lines appearing in all figures in this section represent the reference masses. The predicted intervals and the reference masses are presented visually on Figures (1), (2), (3) and (4), where the first one is for GRS 1915+105, the next two figures – for XTE 1550-564, and the last one is GRO 1655-40. The two figures for XTE 1550-564 represent the results obtained with $\nu_{\text{LF}}^{\text{obs}} = 10$ Hz and $\nu_{\text{LF}}^{\text{obs}} = 18$ Hz, respectively. The numerical values for the masses and spins are given in Table 3.

Some general properties of the models are seen immediately. For the prograde version of the models the RP2 allows the biggest mass tolerance, while the 3:2 K models is the most restrictive. The results clearly indicate that for retrograde orbits not a single model is in agreement with the values obtained by other researchers. We should note that in the retrograde version of the models the constraints on the mass are much narrower than those corresponding

[t]
Table 3. Bounds on the mass and spin

Model	retrograde		prograde	
	a_{\min}	M/M_{\odot}	a_{\min}	M/M_{\odot}
GRS 1915+105				
3:2	0.20	3.2 – 4.7	0.16	5.9 – 17.8
3:1	0.49	6.7 – 8.4	0.29	13.6 – 24.0
2:1	0.60	7.8 – 9.3	0.33	16.6 – 29.6
3:2 K	0.20	3.3 – 4.7	0.16	5.8 – 12.7
RP, 3:1 K	0.47	6.4 – 8.2	0.30	14.0 – 44.6
TD, 2:1 K	0.60	7.7 – 9.2	0.33	16.7 – 41.4
RP1	0.52	7.2 – 8.7	0.28	12.9 – 22.0
RP2	0.43	5.6 – 7.9	0.32	15.5 – 75.6
WD	0.60	7.7 – 9.2	0.33	16.7 – 41.4
XTE 1550-564				
3:2	0.23	2.0 – 2.9	0.17	3.7 – 11.2
3:1	0.55	4.0 – 4.9	0.31	8.3 – 14.9
2:1	0.66	4.6 – 5.4	0.35	10.1 – 26.3
3:2 K	0.22	2.1 – 2.9	0.17	3.7 – 8.0
RP, 3:1 K	0.53	3.9 – 4.8	0.31	8.6 – 26.8
TD, 2:1 K	0.66	4.6 – 5.4	0.35	10.1 – 24.3
RP1	0.59	4.4 – 5.1	0.30	7.9 – 13.3
RP2	0.48	3.4 – 4.6	0.34	9.6 – 45.9
WD	0.66	4.6 – 5.4	0.35	10.1 – 24.3
GRO 1655-40				
3:2	0.13	1.2 – 1.9	0.11	2.2 – 6.9
3:1	0.51	2.5 – 3.1	0.30	5.1 – 9.1
2:1	0.62	2.8 – 3.4	0.34	6.1 – 16.1
3:2 K	0.22	1.3 – 1.8	0.17	2.2 – 4.9
RP, 3:1 K	0.50	2.4 – 3.0	0.31	5.2 – 16.4
TD, 2:1 K	0.62	2.8 – 3.4	0.34	6.1 – 14.9
RP1	0.55	2.7 – 3.2	0.29	4.8 – 8.1
RP2	0.45	2.1 – 2.9	0.33	5.8 – 30.5
WD	0.62	2.8 – 3.4	0.34	6.1 – 14.9

to prograde rotation. In the former case the width of the mass intervals, hence the significance of the estimated values of the mass, is comparable to that of the reference masses. The width of the gap between the segments representing the mass constrains for retrograde and prograde rotation does not depend on the length of the segments.

Bellow we give more details only for the results obtained with the assumption that the orbits are prograde.

4.1 GRS 1915+105

Two of the models impose upper bound on the spin of the black holes which is lower then the maximum allowed by the theory. The RP2 model allows no solutions for spins greater than $a = 0.95$ and the 2:1 model gives solutions only for $a \leq 0.835$.

The masses predicted by the different models for this black hole are in the range $3.2 \leq M/M_{\odot} \leq 75.6$. The retrograde version of the 3:2 model predicts the lowest value, $3.2M_{\odot}$, while the RP2 model, in its prograde version, gives the maximum value for the mass $75.6M_{\odot}$. Two of the models distinctly satisfy the predicted in the literature diapason in their prograde version – 3:2 and 3:2 K. The rest of them do not cover this range even partly. The model 3:2 K pro-

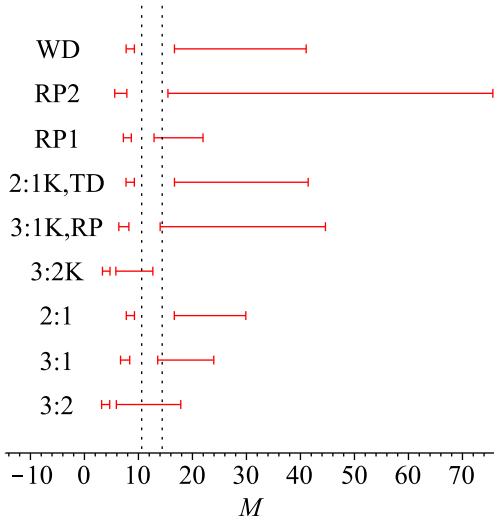


Figure 1. Mass bounds for GRS 1915+105 for retrograde (left segments) and prograde (right segments) orbits. The models are designated on the left. The dotted lines represent the reference masses.

vides the shortest value range, $5.8 \leq M/M_{\odot} \leq 12.7$. The region in which the predictions of the models overlap is $16.7 \leq M/M_{\odot} \leq 17.9$. It does not even remotely coincides with the reference interval $10.6 \leq M/M_{\odot} \leq 14.4$.

4.2 XTE 1550-564

The situation with XTE 1550-564 is a bit more complex than the previous one since we have found two possible maximum values of its LF QPOs in the literature, as it was mentioned in the Introduction. We have done the some calculations twice, for $\nu_{\text{LF}}^{\text{obs}} = 10$ Hz and $\nu_{\text{LF}}^{\text{obs}} = 18$ Hz.

As for the previous black hole the RP2 model allows no solutions for spins greater than $a = 0.95$.

The masses predicted by the different models are in the range $2.0 \leq M/M_{\odot} \leq 49.8$ and coincide for both cases $\nu_{\text{LF}}^{\text{obs}} = 10$ Hz and $\nu_{\text{LF}}^{\text{obs}} = 18$ Hz as the lower and the upper mass limits come from the requirement $a \leq 1$, which yields a lower mass bound in the case of retrograde rotation and an upper mass bound for the case of prograde rotation, and are thus independent of ν_{LF} . The model 3:2 gives the lowest value of the mass: $2.0M_{\odot}$. The model RP2 gives the maximum value: $49.8M_{\odot}$. For $\nu_{\text{LF}}^{\text{obs}} = 10$ Hz five of the nine models cover the entire reference range in the prograde case but give wider mass intervals – 3:2; 3:1; 3:1 K, RP; RP1 and RP2. Among them RP1 gives the narrowest mass range $7.4 \leq M/M_{\odot} \leq 13.3$, which is several times greater than that cited in Table 1 – $8.5 \leq M/M_{\odot} \leq 9.7$. The 3:2 K model does not give solutions in the range obtained by other authors. The bounds given by the 2:1 model only partially overlap with the reference range. The models 2:1K, TD and WD yield the same bounds on the mass which, again, overlap only partially with the reference interval. The zone of simultaneous coverage of all the models is $9.1 \leq M/M_{\odot} \leq 11.2$. It covers only partly the reference interval $8.5 \leq M/M_{\odot} \leq 9.7$.

The greater value of the low frequency, $\nu_{\text{LF}}^{\text{obs}} = 18$ Hz, causes the intervals of possible masses to shorten – the upper

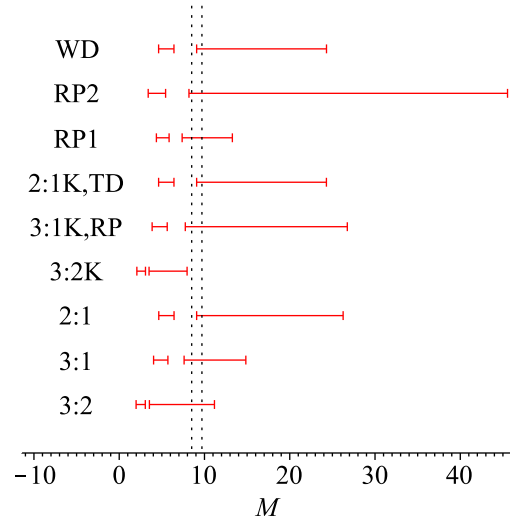


Figure 2. Mass bounds for XTE 1550-56 for retrograde (left segments) and prograde (right segments) orbits. On this figure $\nu_{\text{LF}}^{\text{obs}} = 10$ Hz. The models are designated on the left. The dotted lines represent the reference masses.

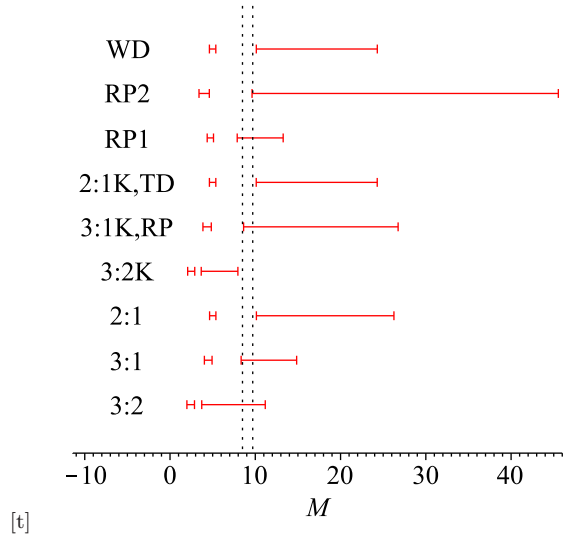


Figure 3. Mass bounds for XTE 1550-56 for retrograde (left segments) and prograde (right segments) orbits. On this figure $\nu_{\text{LF}}^{\text{obs}} = 18$ Hz. The models are designated on the left. The dotted lines represent the reference masses.

bound moves to the left in the retrograde case and the lower bound moves to the right in the prograde case. For $\nu_{\text{LF}}^{\text{obs}} = 18$ Hz for prograde motion four of the nine models entirely cover the range given in Table 1, but predict larger diapason of masses – 3:2; 3:1; 3:1 K; RP and RP1. RP1 again has the shortest range of values – $7.9 \leq M/M_{\odot} \leq 13.3$, which is also much wider than the reference interval – $8.5 \leq M/M_{\odot} \leq 9.7$. Models 2:1; 3:2 K; 2:1 K, TD; RP2 and WD, do not cover the reference range even partly. The zone of simultaneous coverage for all of the models is $10.1 \leq M/M_{\odot} \leq 11.2$, which is half of the diapason for $\nu_{\text{LF}}^{\text{obs}} = 10$ Hz but does not cover the reference interval $8.5 \leq M/M_{\odot} \leq 9.7$ even partly.

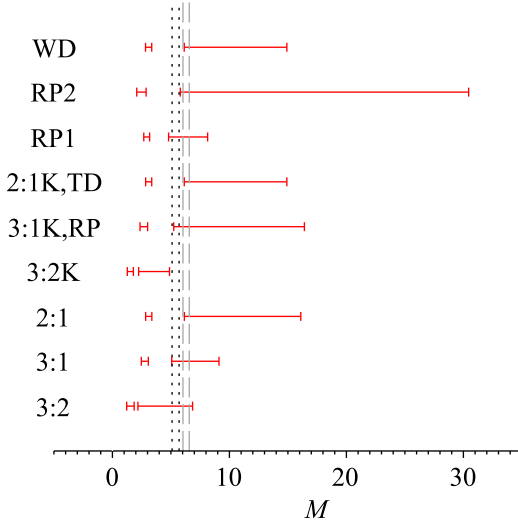


Figure 4. Mass bounds for GRO 1655-40 for retrograde (left segments) and prograde (right segments) orbits. The models are designated on the left. The dotted lines represent the reference masses. The alternative reference mass interval is given by the dashed gray line.

4.3 GRO 1655-40

Here, the RP2 model allows no solutions for spins greater than $a = 0.96$. The masses predicted by the different models are in the range $1.2 \leq M/M_\odot \leq 30.5$. The 3:2 model predicts again the lowest value for the mass: $1.2M_\odot$. The model RP2 gives the maximum value for the mass $30.5M_\odot$. There are two intervals of mass in the literature, $5.1 \leq M/M_\odot \leq 5.7$ and $6.03 \leq M/M_\odot \leq 6.57$. For prograde motion four of the nine models provide a mass interval overlapping with the range obtained by other authors but the – 3:2; 3:1; 3:1 K, RP and RP1. From them RP1 shows the shortest value range – $4.80 \leq M/M_\odot \leq 8.14$. The mass interval for RP2 satisfies only the second reference interval. The 2:1 and 3:2 K model give no solution in the reference range. Models 2:1 K, TD and WD predict identical mass intervals which, however, do not match those in the literature. The zone of simultaneous coverage i.e. the zone in which all models work is $6.15 \leq M/M_\odot \leq 6.85$ i.e. it nearly coincides with the second reference interval $6.03 \leq M/M_\odot \leq 6.57$.

5 QUALITY OF THE MODELS

In the current section⁶ we propose a simple method to estimate the quality of the models. We would like to know what is the average success of the models. What do we mean by “average success”? Each of the models provides an interval of values for the masses of the observed objects. It appears that the prediction of a given model and the mass obtained

through dynamical measurement are in agreement in some cases and in conflict in others. One might ask, which situation is more likely to occur? Is a given model more likely to provide correct mass bounds or not? Can failures be attributed to random errors or are they systematic and should be treated as an indication of a bad model? In the current section we propose a simple statistical approach to this problem which allows us to identify the models for which the discrepancies between predictions and observations are either too big or too frequent.

In a typical situation we would have a sample of experimental values for the mass of a given object. The sample mean is taken as the best estimate of the mass. Here, we are confronted with a different situation. We have one measurement for each of the three objects. Their average does not give us any useful information. We suggest, however, that there is something that the three objects, and all other objects which display HF QPOs in 3:2 ratio and LF QPOs in their X-ray spectra, might have in common and that can be averaged – the relative position of their reference (or observed) mass in the interval of masses that a given model for the HF QPOs provides for them.

Let us explore this idea in more details. We make the hypothesis that the models which we want to test should show some tendency. The reference masses of all three of the objects are to the left of the center of the interval coming from the RP model, for example. Our aim is to find the tendencies that the different models exhibit. In other words we would like to know whether a given model is more likely to underestimate or overestimate the masses of the objects. In which part of the interval do the observations occur most frequently? Is there such point in the interval that “attracts” the observations? These questions can be expressed in a more formal way. Are all masses in the interval provided by a given model equally probable? What is the probability distribution of the values in the interval? Which of the values in the interval gives the best estimate of the mass? Since the probability distribution of the masses is not known we resort to statistics and averaging.

5.1 Rescaled masses

In order to allow averaging we project the mass intervals that a given model provides for the three objects on the unit interval through the following translation

$$m = \frac{M - M_l}{\Delta M}, \quad (9)$$

where M_l and M_u are, respectively, the lower and the upper mass bounds and $\Delta M = M_u - M_l$. For $M \in [M_l, M_u]$ the new variable m varies in the interval $[0, 1]$. The relative positions, or coordinates, of the observed masses are defined as $m_{\text{obs}} = m(M^{\text{obs}})$. They take values in the interval $[0, 1]$ only when $M^{\text{obs}} \in [M_l, M_u]$. The cases $m_{\text{obs}} < 0$ and $m_{\text{obs}} > 1$ indicate a conflict between the prediction of the given model and the observed mass of the object. The unit intervals and the relative positions of the observed masses for all of the studied models are presented in Figure 5. The successful hits are easily recognizable.

⁶ Here, in order to reduce the number of possible scenarios we work with $\nu_{\text{LF}}^{\text{obs}} = 18$ Hz for XTE 1550-56 and then briefly comment on the effect that the alternative choice, $\nu_{\text{LF}}^{\text{obs}} = 10$ Hz, would have on the conclusions. For GRO 1655-40 we work with $5.4 \pm 0.3M_\odot$. The role that an alternative value, e.g. $6.30 \pm 0.27M_\odot$, might have is commented on in subsection 5.4.

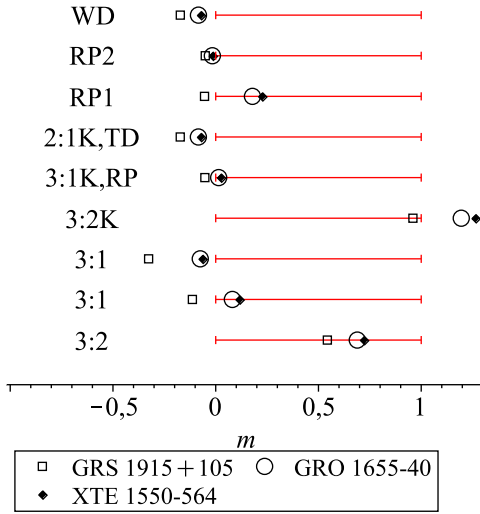


Figure 5. The unit intervals and the relative positions of the observed masses of the objects for all of the studied models.

5.2 Sample mean and sample variance

Let us suppose that we could add more and more objects that share common properties to our sample. Then the values of m_{obs} would span an interval which would coincide with the unit interval in the ideal case⁷. Since no model is perfect the two intervals would not overlap completely. Significant discrepancy between the prediction and the observations would be an indication of a bad model. Let us assume that the expectation value of m_{obs} , i.e. the population mean $\mu_{m_{\text{obs}}}$, was known. It represents the average prediction of a given model. The inverted transformation (9) allows us to find the best estimate of the mass: $M_{\text{best estimate}} = M(\mu_{m_{\text{obs}}})$. If $\mu_{m_{\text{obs}}} < 0$ or $\mu_{m_{\text{obs}}} > 1$ then the model tends to, respectively, overestimate or underestimate the masses of the objects. In case $\mu_{m_{\text{obs}}} = 0.5$ the model is in complete agreement with the observations. Since the population is unknown we will work with the available sample which consists of only three objects.

The average relative position \bar{m}_{obs} ⁸, i.e. the sample mean, serves as an estimate of the population mean $\mu_{m_{\text{obs}}}$, $\hat{\mu}_{m_{\text{obs}}} = \bar{m}_{\text{obs}}$ as usual. The sample's standard deviation $s_{m_{\text{obs}}}$ shows how strong the tendency that the models reveal is. Small values of $s_{m_{\text{obs}}}$ mean that all the observations group in a narrow interval. The standard error of the sample mean (SEM), which tells us how far is the sample mean likely to be from the population mean, is given by $s_{m_{\text{obs}}}/\sqrt{N}$, where $N = 3$ in our case.

The results from the averaging of these quantities over the available sample of three objects for each of the nine studied models is given in Table 4. The models are listed in the first column. Column two represents the sample mean

⁷ m_{obs} would cover the entire unit interval, if the spin of the black hole which has produced a give set of values for the HF and LF QPOs could take any value in the interval $[a_{\text{min}}, 1]$.

⁸ See appendix B for this and all other formulas in the current section.

[t]

Table 4. Statistics

Model	$\bar{m}_{\text{obs}} \pm \text{SEM}$	$s_{m_{\text{obs}}}$	$\sigma \bar{m}_{\text{obs}}$
3:2	0.65 ± 0.05	0.09	0.09
3:1	0.03 ± 0.07	0.12	0.10
2:1	-0.16 ± 0.09	0.15	0.05
3:2 K	1.14 ± 0.09	0.16	0.16
RP, 3:1 K	-0.004 ± 0.02	0.04	0.04
TD, 2:1 K	-0.11 ± 0.03	0.05	0.05
RP1	0.11 ± 0.09	0.15	0.12
RP2	-0.03 ± 0.01	0.02	0.02
WD	-0.11 ± 0.03	0.05	0.05

and its standard error, and the standard deviation of the experimental points is in the third column.

5.3 Viability of the models

The models for which the sample mean is outside of the unit interval even when the SEM is taken into account, i.e. they are in clear conflict with the observations, are marked in bold. The third column of Table 4 reveals that the tendencies are rather strong since the scatter of the points is only 16% at most (See the data for model 3:2 K.). As it can be seen, our results disfavor five of the nine groups of models: 2:1; 3:2 K; TD, 2:1 K; RP2; WD. The viable models in decreasing order of their quality⁹ are: 3:2; RP1; 3:1 and RP, 3:1 K.

5.4 The effect of uncertainties in the reference masses

A reference in the literature shows that over the years the values of the masses of the central object in the studied microquasars change. They might vary significantly from one study to the other. We refer the reader to (Reid et al. 2014) and (Steehgs et al. 2013) for different estimates of the mass of GRS 1915+105, and to (Beer & Podsiadlowski 2002) and (Orosz 2003) for different estimates of the mass of GRO 1655-40, for example.

With this in mind, we evaluate the effect that uncertainties in the reference masses $\sigma_{M_{\text{obs}}}$ have on the results given in the second column of Table 4, which are the basis for our conclusions about the viability of the models. Variance within one Solar mass, i.e. $\sigma_{M_{\text{obs}}} = 1M_{\odot}$, for all of the three microquasars is reasonable. The results for the uncertainties of the average positions of the observed masses $\sigma \bar{m}_{\text{obs}}$ are given in the last column of Table 4.

Combined unfavorable contribution of SEM and $\sigma \bar{m}_{\text{obs}}$ would have no effect on the conclusion concerning the viability of the following models: 3:2; 2:1; TD, 2:1 K; WD. The possibility that errors could change the conclusions about

⁹ Here, by quality we mean the distance of the average position from the center of the interval – the smaller the distance, the greater the quality. Once $\mu_{m_{\text{obs}}}$ corresponding to a given model is known we can apply it to obtain the best estimate of the mass, even if the model demonstrates poor quality. We would know what correction should be made in the prediction coming from the model in question. Loosely speaking, $|\mu_{m_{\text{obs}}} - 1/2|$ is the bias of the models.

the other five groups of model – 3:1; 3:2 K; RP, 3:1 K; RP1; RP2 – cannot be discarded.

6 CONCLUSION

The mass bounds that the different models impose on the masses of the objects provide a unequivocal proof that the central object in all three of the studied LMXBs is a black hole. An exception from this observation are the mass estimates given by the retrograde version of the 3:2 and the 3:2 K models about GRO 1655-40.

For all three of the objects the bounds on the mass resulting from the retrograde version of the models are much more tight than those coming from the prograde version. The severe conflict between the latter and the reference values for the masses of the objects imply that retrograde motion of matter in the accretion disk is highly unlikely.

Two of the models, 3:2 and 3:2 K, show systematic tendency to underestimate the masses of the objects. Their best estimates are lower than the center of the reference intervals in all three of the cases. On the contrary, the rest of the models seem to overestimate the masses of the studied objects. Relatively moderate mass bounds, neither too high nor too low, are provided by the following set of models – 3:2; 3:1; RP1. These models appear to be favored by the current study.

Of all the models the 3:2 K and the RP1 are the most restrictive and still the predictions of the latter are rather acceptable¹⁰. The RP2 model is the least restrictive when it comes to the masses. When it comes to the spin, however, in all of the cases it poses a upper bound which is lower than the highest admissible theoretical value $a = 1$.

With a few exceptions, the lower bound on the specific angular momentum of the central object that a given model imposes, a_{\min} , varies slightly from one object to the other.

The statistical approach for the assessment of the average success of the models reveals that conflicts the mass bounds provided by the following models: 2:1; 3:2 K; 2:1 K, TD; RP2 and WD, on the one side, and the reference masses, on the other side, occur more often than not. The viable models, in increasing order of their quality, are: 3:2; RP1; 3:1 and RP, 3:1 K.

The conclusions based on the averaging of the observations for the three microquasars are sensitive to our knowledge of the precise values of the reference masses (denoted here as M^{obs}). For uncertainties lower than or at most equal to one Solar mass our conclusions for 3:2; 2:1; TD, 2:1 K; WD would not be affected.

ACKNOWLEDGEMENTS

I.S. would like to thank his wife for the support, Dr. Sava Donkov for reading the manuscript and for the numerous discussions on the subject, prof. Stoytcho Yazadjiev for drawing his attention to the subject of quasiperiodic oscillations of black holes and neutron stars.

¹⁰ The more restrictive a given model is, the more likely a conflict with the referential interval is to occur.

REFERENCES

- Abramowicz M. A., Kluzniak W., 2004, AIP Conference Proceedings **714**, 21
- Abramowicz M. A., Kluzniak W., Stuchlik Z., Török G., 2004, arXiv:astro-ph/0401464
- Aliev A. N. and Gal'tsov D. V., 1981, Gen. Relat. Gravit. **13**, 899
- Aliev A. N., Gal'tsov D. V. and Petukhov V. I., 1986., Astr. Space Sci. **124**, 137
- Aliev A. N., Esmer G. D., Talazan P., 2013, Class. Quantum Grav. **30**, 045010
- Altamirano D., Ingram A., van der Klis M., Wijnands R., Linares M., Homan J., 2012, ApJ **759**, L20
- Bambi C., 2012, JCAP **1209**, 014
- Bambi C., 2015, Eur. Phys. J. C **75**, 162
- Beer M.E., Podsiadlowski P., 2002 MNRAS **331**, 351
- Belloni T., Psaltis D., van der Klis M., 2002, ApJ **572**, 392
- Blum J. L., Miller J. M., Fabian A. C., Miller, et al., 2009, ApJ **706**, 60
- Bursa M., 2005, In Proceedings of RAGtime 6/7, Opava, editors S. Hledik and Z. Stuchlik
- Cadez A., Calvani M., Kostic U., 2008, A & A **487**, 527
- Casella P., Belloni T., Stella L., 2005, ApJ **629**, 403
- Franchini A., Motta S.E., Lodato G., 2017, MNRAS **467**, 145
- Germana C., Kostic U., Cadez A., Calvani M., 2009, AIP Conf.Proc. **1126**, 367
- Hurley D. J., Callanan P. J., Elebert P., Reynolds M. T., 2013, MNRAS **430**, 1832
- Kato S., 2004a, PASJ, 56, 559
- Kato S., 2004b, PASJ, 56, 905
- Kato S., 2004c, PASJ, 56, L25
- Kato S., 2005a, PASJ, 57, L17
- Kato S., 2005b, PASJ, 57, 679
- Kato S., 2007, PASJ, 59, 451
- Kato S., 2008, PASJ, 60, 889
- Kostic U., Cadez A., Calvani M., Gomboc A., 2009, A&A, 496, 307
- Lin Y.F., Boutelier M., Barret D., Zhang S. N., 2011, ApJ **726**, 12
- McClintock J. E., Remillard R. A., 2006a, in Compact Stellar X-Ray Sources, ed. W. H. G., Lewin & M. van der Klis (Cambridge: Cambridge Univ. Press), 157, arXiv:astro-ph/0306213
- McClintock J. E., Shafee R., Narayan R., Remillard R. A., Davis S. W. and Li L. -X., 2006b ApJ **652**, 518, arXiv:astro-ph/0606076
- Merloni A., Vietri M., Stella L., Bini D., 1999, MNRAS, **304**, 155
- Middleton M., Done Ch., Gierlinski M., Davis Sh., 2006, MNRAS **373**, 1004, arXiv:astro-ph/0601540
- Morgan E. H., Remillard R.A., and Greiner J., 1997, ApJ **482**, 993
- Motta S. E., Belloni T. M., Stella L., Munoz-Darias T., Fender R., 2014a, MNRAS **437**, 2554
- Motta S. E., 2016, AN, **337**, 398, arXiv:1603.07885
- Orosz J. A., 2003, in IAU Symp. 212, A Massive Star Odyssey: From Main Sequence to Supernova, ed. K. van der Hucht, A. Herraro, & C. Esteban, p. 365
- Orosz J. A., Steiner J. F., McClintock J. E., Torres M. A. P., Remillard R. A., Bailyn C. D., Miller J. M., 2011, ApJ **730**, 13
- Pasham D. R., Cenko S. B., Zoghbi A., Mushotzky R. F., Miller J., Tombesi F., 2015, ApJ **811**, 8
- Rebusco P., 2008, New Astron. Rev. **51**, 855, arXiv:0801.3658
- Reid M. J., McClintock J. E., Steiner J. F., Steeghs D., Remillard R. A., Dhawan V., Narayan R., 2014, ApJ **796**, 8
- Remillard R.A., Morgan E.H., McClintock J.E., et al., 1999, ApJ **522**, 397
- Remillard R. A., Sobczak G. J., Muno M. P., McClintock J. E., 2002a, ApJ **564**, 962, arXiv:astro-ph/0105508

- Remillard R. A., Muno M. P., McClintock J. E. and Orosz J. A., 2002b, *ApJ* 580, 1030, [astro-ph/0202305].
- Remillard R. A., McClintock J. E., 2006a, *Ann. Rev. Astron. Astrophys.*, 44, 49, [astro-ph/0606352]
- Schnittman J. D., Homan J., Miller J. M., 2006, *ApJ*, 642, 420
- Shafee R., McClintock J. E., Narayan R., Davis S. W., Li L. -X. and Remillard R. A., 2006, *ApJ* 636, L113
- Sobczak G. J., McClintock J.E., Remillard R. A., Cui W., Levine A. M., Morgan E. H., Orosz J. A., Bailyn, C.D., 2000, *ApJ* 531, 537, arXiv:astro-ph/9910519
- Steehls D., McClintock J.E., Parsons S.G., Reid M.J., Littlefair S., Dhillion V.S., 2013, *ApJ* 768, 185
- Stefanov I. Zh., 2014, *MNRAS* 444, 2178
- Stefanov I. Zh., 2016, *Astron. Nachr.* 337, 246
- Stella L., Vietri M., 1998, *ApJ* 492, L59
- Stella L., Vietri M., Morsink S., 1999, *ApJ* 534, L63
- Strohmayer T. E., 2001, *ApJ*, 552, L49, [astro-ph/0104487]
- Stuchlik Z., Konar S., Miller J. C., Hledik S., 2008, *A&A*, 489, 963
- Stuchlik Z., Kotrlova A., 2009, *GRGr*, 41, 1305
- Stuchlik Z., Schee J., 2012, *CQGGr*, 29, 065002
- Stuchlík Z., Kološ M., 2016a, *ApJ* 825, 9
- Stuchlík Z., Kološ M., 2016b, *A&A* 586, 6
- Török G., Abramowicz M. A., Kluzniak W., Stuchlik Z., 2006, *AIP Conf. Proc.*, 861, 786, arXiv:astro-ph/0603847
- Török G., Abramowicz M. A., Stuchlík Z., Šrámková E., 2007, *Binary Stars as Critical Tools & Tests in Contemporary Astrophysics*, Proceedings of IAU Symposium #240, held 22-25 August, 2006 in Prague, Czech Republic. Edited by W.I. Hartkopf, E.F. Guinan and P. Harmanec. Cambridge: Cambridge University Press, 724, arXiv:astro-ph/0610497
- Török G., Bakala P., Šrámková E., Stuchlík Z., Urbanec M.: 2010, *ApJ* 714, 748
- Török G., Kotrlová A., Šrámková E., Stuchlík Z., 2011, *A&A*, 531, A59
- Török G., Bakala P., Šrámková E., Stuchlík Z., Urbanec M., Goluchová K., 2012, *ApJ* 760, 15
- Török G., Goluchová K., Urbanec M., Šrámková E., Adámek K., Urbancová G., Pecháček T., Bakala P., Stuchlík Z., Horák J., Juryšek J., 2016, *ApJ* 833, 11, arXiv:1611.06087
- van Doesburgh M., van der Klis M., 2017, *MNRAS* 465, 3581
- van der Klis M., 2006, in *Compact Stellar X-Ray Sources*, ed. W. H. G., Lewin & M. van der Klis (Cambridge: Cambridge Univ. Press), 39, arXiv:astro-ph/0410551
- Zhang S. N., 2013, *Frontiers of Physics*, 8, 630, arXiv:1302.5485
- Zhou X. L., Yuan W., Pan H. W., Liu Z., 2015, *ApJ* 798, 4

APPENDIX A: EPICYCLIC FREQUENCIES

The explicit form of the orbital frequency ν_ϕ and the two epicyclic frequencies – the radial ν_r and the vertical ν_θ – for the Kerr black hole have been obtained for the first time in (Aliev & Gal'tsov 1981; Aliev et al. 1986) but can be found also, for example, in (Aliev, Esmer & Talazan 2013)

$$\nu_\phi = \left(\frac{c^3}{2\pi GM} \right) \frac{1}{r^{3/2} \pm a}, \quad (\text{A1})$$

$$\nu_r^2 = \nu_\phi^2 \left(1 - \frac{6}{r} - \frac{3a^2}{r^2} \pm \frac{8a}{r^{3/2}} \right), \quad (\text{A2})$$

$$\nu_\theta^2 = \nu_\phi^2 \left(1 + \frac{3a^2}{r^2} \mp \frac{4a}{r^{3/2}} \right). \quad (\text{A3})$$

The upper (lower) sign corresponds to prograde (retrograde) direction of rotation of the hot spot¹¹. In this paper all the masses are scaled with the Solar mass, the radii are scaled with the gravitational radius $r_g \equiv GM/c^2$, and the specific angular momentum $a \equiv J/cM^2$ is used.

APPENDIX B: STATISTICAL FORMULAS

The formulas for the sample mean \bar{m}_{obs} and the sample standard deviation $s_{m_{\text{obs}}}$ are:

$$\bar{m}_{\text{obs}} = \frac{1}{N} \sum_{i=1}^N m_{\text{obs},i}, \quad (\text{B1})$$

$$s_{m_{\text{obs}}} = \sqrt{\frac{1}{N-1} \sum_{i=1}^N (\bar{m}_{\text{obs}} - m_{\text{obs},i})^2}. \quad (\text{B2})$$

In order to obtain the uncertainty of the average position of the observed masses $\sigma_{\bar{m}_{\text{obs}}}$ which is due to the uncertainties of the observed (reference) masses $\sigma_{M_i^{\text{obs}}}$ we apply a standard uncertainty propagation formula:

$$\begin{aligned} \sigma_{\bar{m}_{\text{obs}}}^2 &= \sum_{i=1}^N \left(\frac{\partial \bar{m}_{\text{obs}}}{\partial M_i^{\text{obs}}} \right)^2 \sigma_{M_i^{\text{obs}}}^2 \\ &= \frac{1}{N^2} \sum_{i=1}^N \frac{1}{\Delta M_i^2} \sigma_{M_i^{\text{obs}}}^2. \end{aligned} \quad (\text{B3})$$

Here the index i enumerates the three microquasars: GRS 1915+105, GRO 1655-40 and XTE 1550-564, and $N = 3$.

This paper has been typeset from a $\text{\TeX}/\text{\LaTeX}$ file prepared by the author.

¹¹ In (Stefanov 2014, 2016) a different convention for the angular momentum has been used. In these papers the spin can take both positive and negative values. A change in the sign of the spin is equivalent to inversion of the direction in which the test particle orbits around the black hole. Here, we work with the magnitude of the spin and in order to change the orientation of an orbit (prograde or retrograde) we have to make the proper choice of the signs in formulas (A1)–(A3).

